A Metal-Only Reflectarray Made of 3D Phoenix Cells

Zhihang An, Tony Makdissy, Maria Garcia Vigueras, Sébastien Vaudreuil, Raphaël Gillard

A Metal-Only Reflectarray Made of 3D Phoenix Cells

Zhihang An[1], Tony Makdissy[2], María Garcia Vigueras[1], Sébastien Vaudreuil[3], Raphaël Gillard[1]
[1] Institute of Electronics and Telecommunications of Rennes, INSA, 35708 Rennes, France, Zhihang.An@insa-rennes.fr
[2] TICKET Research Laboratory, Antonine University, 40016 Hadat-Baadba, Lebanon
[3] Euromed University of Fes, 51 30 030 Fès, Morocco

***Abstract*—This paper presents a metal-only reflectarray antenna made of 3D phoenix cells and its fabrication using additive manufacturing. An electric circuit is proposed for analyzing the behavior and capabilities of the considered cell. The agreement between full-wave simulations and the circuit predictions is very satisfactory when varying the cell geometrical parameters on a large range of values. The simulated gain of the designed reflectarray at 20 GHz is 30.2 dBi with an efficiency of 49.3% and a 1 dB-gain bandwidth of 17.5%. The proposed reflectarray is suitable for working in severe environments due to its metal-only characteristics.**

***Index Terms*— reflectarray antenna, 3D phoenix cell, metal–only.**

I. INTRODUCTION

Reflectarray antennas (RAs) can be seen as a combination of planar arrays and parabolic reflectors with the advantages of high gain, low profile, low cost and easy manufacturing. The most common RA is implemented in microstrip technology, which consists of metallic resonators printed on a dielectric substrate backed by a ground plane. However, the use of such dielectric materials may limit their gain due to the losses they bring, especially at high frequencies. In addition, for RAs that work in harsh environment, such as space, the use of dielectric substrates is not recommended due to undesired associated effects. In such a situation, the metal-only reflectarray (MORA) is preferred as it avoids the intrinsic problems brought by dielectric materials such as outgassing and temperature-dependent dielectric constant. The simplest MORA that can be identified in the literature involves the use of one or more metal sheets with slot apertures [1-2]. Thanks to the additional degrees of freedom they offer, actual 3D structures provide more flexibility for achieving a full 360° phase-range and advanced functionalities. In [3] and [4], metal grooves or metal blocks of variable height have thus been used to control the reflection phase. These MORA were fabricated with micromachining technology. Additive manufacturing offers even more possibilities to fabricate complex MORA cells. A few examples have been reported using material jetting where a 3D-printed plastic structure is coated with metal [5].

To the best knowledge of the authors, there has been no MORA fabricated using SLM (Selective Laser Melting) yet. SLM is very attractive because the metal particles can hold together without using any additional supporting material [6]. In a previous paper, we demonstrated that the 3D phoenix cell (PC) can be fabricated using SLM [7]. This new cell preserves the unique capability to loop back to its initial state after a complete phase cycle and provides additional degrees of freedom (in comparison with its microstrip counterpart) to control the reflection phase. In the present paper, we propose a more complete description of its behavior using an electric circuit (section II) and we present its application in a real MORA (section III).

II. 3D PHOENIX CELL & EQUIVALENT CIRCUIT

A. Cell Description

The concept of PC was originally presented in [8] as a dual-polarization microstrip cell with a 360° phase range over a large frequency range and the unique property to come back to its initial geometry after a complete phase cycle. A metal only (MO) version of the PC was then proposed in [2] using slots in a metal sheet. Unfortunately, since the dielectric layer was removed, there was no support anymore for the isolated metal elements and a connecting strip was needed to attach them to the sheet. As a consequence, the PC lost in this case its 90° rotational invariance and subsequently its capability to deal with dual polarization. Finally, a 3D MO PC has been recently designed, fabricated and measured in [7]. For this 3D PC, the metal rings are replaced by square waveguides. Since the waveguides don't need anything else to support themselves, the 3D PC recovers the rotational invariance. Therefore, it is a dual-linearly polarized PC and it is selected in this paper to design the 3D MORA.

As shown in Fig.1, the 3D PC consists of two concentric square metallic waveguides and a square metallic block at the center. The metallic block is used to reduce the cutoff frequency of the waveguides and make their cross-section more compact in order to avoid the excitation of Floquet harmonics in the array. As for the original PC, the reflection phase is controlled by parameter L_r, which is here the size of the inner waveguide. Moreover, the height h can offer an additional degree of freedom as shown in [7]

At the initial stage (Fig.2), the size of the inner waveguide is equal to the size of the central metallic block (which means there is no inner waveguide). The inner waveguide then appears as L_r increases. At the final stage, L_r is equal to L_c and the inner waveguide disappears again. The cell thus comes back to its initial geometry.

The 3D PC is simulated using HFSS®. It is assigned perfect electric conductor boundary on the metallic surface. During the simulation, the Floquet port is used and the

master/slave boundary condition is assigned on the lateral faces to mimic a cell in a periodic infinite environment. Table I summarizes the detailed parameters of the 3D PC. The size of the outer waveguide (L_c) is set to 7.5 mm ($\lambda_0/2$ at 20 GHz) in order to avoid grating lobes. The height (h) is in the range from 0-10 mm, which is enough to generate a complete phase cycle. Since two adjacent cells in the RA share the same wall, the considered thickness of the outer waveguide is half that of the inner waveguide.

The simulated reflection phase at 20 GHz is shown in Fig.3. The complete 360° phase-range can easily be achieved when h is greater than 4 mm, which will be explained by the equivalent circuit in the next subsection. The plot clearly shows it is possible to use both h and L_r to tune the phase.

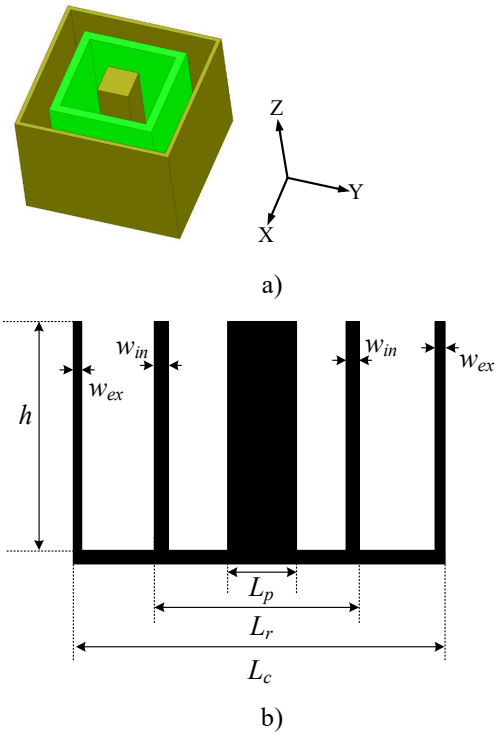

Fig. 1. a) The 3D PC. b) The sectional view of 3D PC

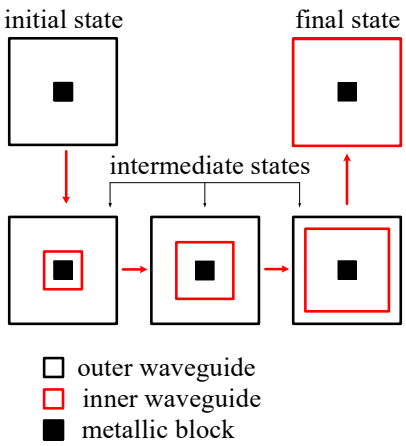

Fig. 2. The variation mechanism of the 3D PC (the top view)

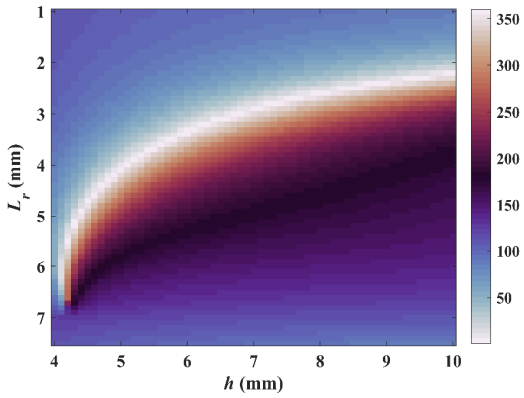

Fig. 3. The reflected phase of the 3D PC at 20GHz versus L_r and h

B. Equivalent Circuit

In order to have a comprehensive understanding of the 3D PC, an equivalent circuit is proposed. As the 3D PC consists of two waveguides, its input impedance mainly depends on their input impedances. In addition, three shunt impedances are used at the entrance of both waveguides to model the discontinuity effects. As a result, the equivalent circuit can be represented as shown in Fig.4. The corresponding input impedance is given by:

$$Z_{input} = \frac{1}{\frac{1}{Z_{disc\_0}} + \frac{1}{\frac{1}{\frac{1}{Z_{in}} + \frac{1}{Z_{disc\_in}}} + \frac{1}{\frac{1}{Z_{ex}} + \frac{1}{Z_{disc\_ex}}}}} \quad (1)$$

where Z_{in} and Z_{ex} are the input impedances of the inner and the outer waveguides respectively, when loaded by a short circuit. Z_{disc_in}, Z_{disc_ex} and Z_{disc_0} are three discontinuity impedances which characterize the reactive excitation of all higher order modes, including higher order modes in the WG and Floquet harmonics, and the coupling between them. Note that the two waveguides are connected in series.

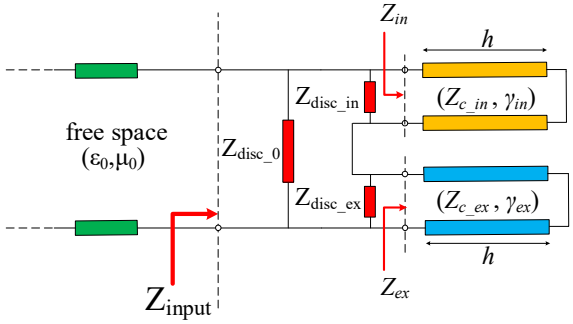

Fig. 4. The equivalent circuit of 3D PC

The waveguides input impedances, Z_{in} and Z_{ex}, can be calculated analytically, for any value of h, using simple transmission line theory. This only requires the preliminary determination of the characteristic impedances and

propagation constants of the waveguides. The derivation of these characteristics relies on one electromagnetic (EM) simulation for each waveguide and for each considered L_r. The discontinuity impedances Z_{disc_in}, Z_{disc_ex} and Z_{disc_0} can also be derived from EM simulations. Once again, the derivation must be repeated for each considered L_r since these discontinuity impedances are strongly affected by the cross-section of the PC. The principle of derivation consists in simulating the whole structure (Fig.1) for three different h values. These simulations yield three different values for Z_{input}. Z_{in} and Z_{ex} are then calculated analytically for the same values of h. Finally, Z_{disc_in}, Z_{disc_ex} and Z_{disc_0} can be solved involving three different equalities established using equation (1). In practice, the three different values used for h are 3.5, 5 and 6.5 mm. Numerical tests have shown that the final results are quite stable when these values are changed.

TABLE I. THE DETAILED PARAMETERS OF THE PC

Parameter	L_c	L_r	L_p	h	w_{in}	w_{ex}
Value	7.5	1-7.5 (step=0.1)	1	0-10 (step=0.1)	0.2	0.1

Figure 5 shows the comparison between the equivalent circuit and full wave simulations for different L_r (L_r is in the range from 1 mm to 7 mm with a step of 1 mm) at 20GHz. The phase error for each considered L_r or h is always less than 11°, which means the agreement between equivalent circuit and full wave simulations is pretty good.

In addition, the proposed equivalent circuit accounts well for the observations made about Fig. 3 (end of section II.A), as will be discussed now.

It can be seen from equation (1) that the reflection phase is controlled by Z_{in}, Z_{ex} and the three discontinuity impedances all together. Z_{disc_in}, Z_{disc_ex} and Z_{disc_0} are mainly determined by L_r. In order to better address the influence of Z_{in} and Z_{ex}, Figure 6 shows the characteristics of both waveguides. Obviously, the outer waveguide always operates in the propagative mode. On the contrary, it can be seen that the inner waveguide always operates under cutoff at the considered frequency (20 GHz). Thus, the reflection phase is mainly affected by Z_{ex} which is jointly determined by the propagation constant, the characteristic impedance and the height of the 3D PC:

$$Z_{ex} = jR_{C\_ex} \tan(\beta_{ex} h) \qquad (2)$$

where R_{C_ex} and β_{ex} represent respectively the real part of the characteristic impedance and the imaginary part of the propagation constant of the outer waveguide. It can be seen from Fig.6 b) that a small L_r (L_r<2 mm) reduces the propagation constant of the outer waveguide while a large L_r reduces its characteristic impedance. Thus, Z_{ex} is small and only weakly affected by h in these cases. As a consequence, the reflection phase remains almost constant, as can be seen in Fig. 3. On the other hand, if h is small, the propagation within the waveguides is almost negligible and the reflection phase is also hardly affected by the characteristics of these waveguides. This is why the reflection phase is almost constant when h is smaller than 4 mm.

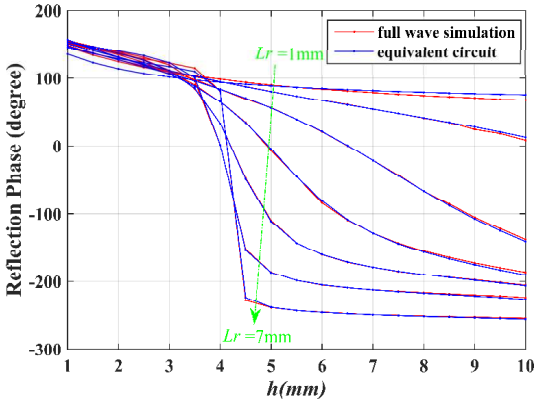

Fig. 5. The reflection phases of the equivalent circuit and full wave simulations.

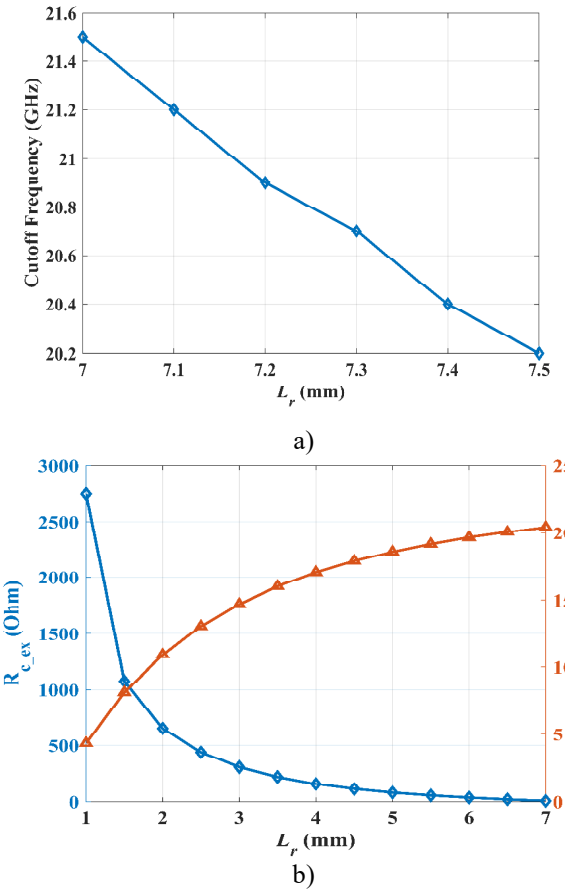

Fig. 6. a) The cutoff frequency of inner waveguide. b) The characteristic impedance and the propagation constant of outer waveguides.

III. REFLECTARRAY DESIGN AND FABRICATION

In order to validate the potential of additive manufacturing at the scale of an array, a MORA was designed and fabricated. The center frequency of the designed RA is 20 GHz. The radiating aperture is $13\lambda_0 \times 13\lambda_0$. The RA is illuminated by a horn antenna with an

offset angle of 25° with respect to the normal of the panel. The f/d ratio is 1.183. The direction of the main beam has a tilt angle of 25° (opposite to the offset).

As shown in Table II, the wall thickness of the 3D PC is adjusted to 0.3 mm to be compliant with the fabrication tolerances. To reduce the profile and provide sufficient phase range, the height of the 3D PC is fixed at 6 mm. During the fabrication, the RA is under the nitrogen atmosphere at 100W/275W (border/volume) laser power (λ=1075 nm). The material used is a 316L stainless steel powder with a diameter distribution between 10 and 45 µm. Figure 7 shows the designed RA with the horn antenna and the fabricated RA respectively.

For the design of the RA, the 3D PC is simulated in HFSS®. A conductivity of 1.33×10^6 S/m is used to represent the real metal material. Since the incident angle of the cells in the center of RA is close to 25° and the cells in the center have stronger illumination intensity, the EM characterization of the cells is carried out for this particular incident angle (and not at normal incidence as it is usually done). Then, the complete designed RA is also simulated in HFSS® together with its illuminating horn antenna. Figure 8 shows the simulated gain in E-plane and the simulated gain versus frequency respectively. It can be seen that the simulated gain at 20 GHz is 30.2 dBi with an antenna efficiency of 49.3% and the side lobe and cross-polarization levels are about 19 dB and 46 dB below the maximum radiation of the main beam respectively. The 1 dB-gain bandwidth is about 17.5% although the design was not optimized for large bandwidth. The detailed design procedure and measurement results will be presented at the conference.

TABLE II. THE DETAILED PARAMETERS OF MODIFIED PC

Parameter	L_c	L_r	L_p	h	w_{ex}	w_{in}
Value	7.5	1-7.5 (step=0.05)	1	6	0.2	0.3

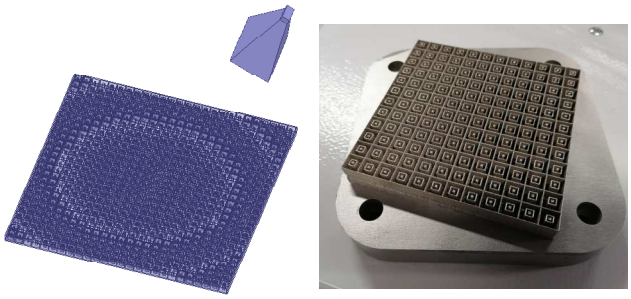

a) b)

Fig. 7. a) The designed RA and horn antenna. b)The fabricated RA.

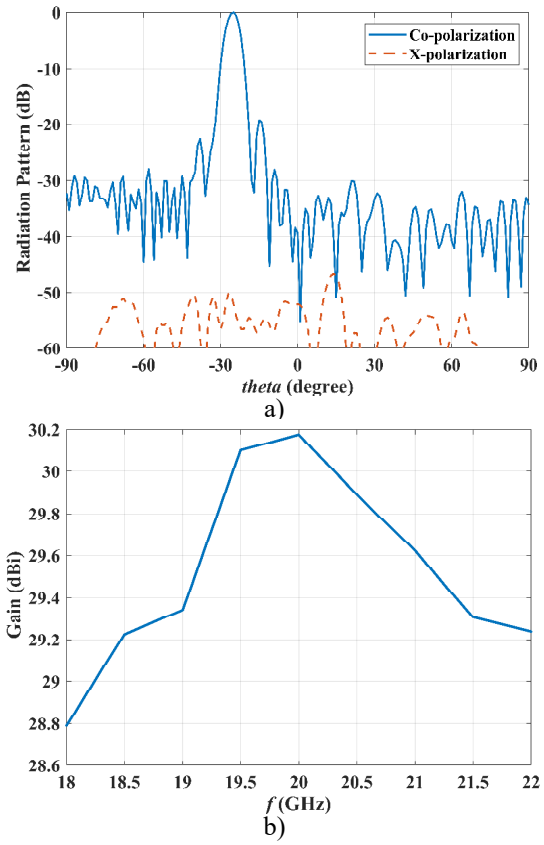

Fig. 8. a) The simulated gain at E-plane at 20 GHz. b) The simulated gain versus Frequency.

IV. CONCLUSION

In this work, a 3D MORA made of PCs is designed and fabricated using additive manufacturing technology for the first time. The 3D PC is analyzed in detail with the use of an equivalent circuit. The phase error between the equivalent circuit and full wave simulation is always less than 11° for each case, which makes it suitable for preliminary design of the RA. The simulated gain of designed RA at 20 GHz is 30.2 dBi with an antenna efficiency of 49.3% and the 1dB-gain bandwidth is about 17.5%.

ACKNOWLEDGMENT

The work was jointly funded by the Agence Universitaire de la Francophonie (Moyen-Orient) and the National Council for Scientific Research Lebanon (CNRS-L).

REFERENCES

[1] W. An, S. Xu and F. Yang, "A Metal-Only Reflectarray Antenna Using Slot-Type Elements," *IEEE Antennas and Wireless Propagation Letters*, vol. 13, pp. 1553-1556, July 2014.

[2] R. Deng, F. Yang, S. Xu and M. Li, "A Low-Cost Metal-Only Reflectarray Using Modified Slot-Type Phoenix Element With 360° Phase Coverage," *IEEE Transactions on Antennas and Propagation*, vol. 64, no. 4, pp. 1556-1560, April 2016.

[3] Y. H. Cho, W. J. Byun and M. S. Song, "High Gain Metal-Only Reflectarray Antenna Composed of Multiple Rectangular Grooves,"

IEEE Transactions on Antennas and Propagation, vol. 59, no. 12, pp. 4559-4568, December 2011.

[4] Deng R, Yang F, Xu S, et al., "A 100-GHz metal-only reflectarray for high-gain antenna applications," . *IEEE Antennas and Wireless Propagation Letters*, vol. 15, 178-181, May 2015.

[5] Chen B J, Yi H, Ng K B, et al., "3D printed reflectarray antenna at 60 GHz," *2016 International Symposium on Antennas and Propagation (ISAP)*, Okinawa, Japan, October 2016.

[6] Harris I D, "Development and implementation of metals additive manufacturing," in *Additive Manufacturing Handbook: Product Development for the Defense Industry*, CRC Press, 1st edition, 2017.

[7] Makdissy T, Gillard R, An Z, et al., "Dual Linearly Polarized 3D Printed Phoenix Cell for Wide Band Metal Only Reflectarrays,". *IET Microwaves, Antennas & Propagation*, vol. 14, no. 12, pp. 1411-1416, June 2020.

[8] Moustafa L, Gillard R, Peris F, et al., "The phoenix cell: A new reflectarray cell with large bandwidth and rebirth capabilities, ". *IEEE Antennas and wireless propagation letters*, vol. 10, pp. 71-74, January 2011.